EFDA–JET–PR(13)62

E. Barbato, A. Saveliev, I. Voitsekhovitch, K.Kirov, M. Goniche,
the ISM ITER Scenario Modeling group
and JET EFDA contributors

Time Dependent Simulation of Lower Hybrid Current Drive in JET Discharges

Time Dependent Simulation of Lower Hybrid Current Drive in JET Discharges

E. Barbato[1], A. Saveliev[2], I. Voitsekhovitch[3], K.Kirov[3], M. Goniche[4],
the ISM ITER Scenario Modeling group
and JET EFDA contributors*

JET-EFDA, Culham Science Centre, OX14 3DB, Abingdon, UK

[1]ENEA, CP 65-00044- Frascati, Rome, Italy
[2]Ioffe Institute, St Petersburg, Russian Federation
[3]EURATOM-CCFE Fusion Association, Culham Science Centre, OX14 3DB, Abingdon, OXON, UK
[4]CEA, IRFM, F-13108 Saint Paul-lez-Durance, France
** See annex of F. Romanelli et al, "Overview of JET Results",*
(24th IAEA Fusion Energy Conference, San Diego, USA (2012)).

Preprint of Paper to be submitted for publication in
Nuclear Fusion

ABSTRACT

In this paper we report on simulations of LHCD in JET closely comparing the simulation results to the available experimental data. The simulations are performed all over the relevant discharge duration by ASTRA. The LHCD module, FRTC, is based on a standard Ray tracing Fokker Planck model. The main purpose of the paper is to understand the present LHCD experiments issues *within the limit of the LH linear propagation model*. Such main issues are: i) analysis of Non Resonant Collisional Absorption (NRCA) of LH wave power at JET during the current ramp up phase and in steady state scenarios, ii) the associated problem of lack of penetration of LHCD in high density plasmas, iii) current diffusion during the LHCD assisted current ramp up and iv) assessment of the current profile alignment in JET Steady State (SS) discharges in the presence of LHCD.

In recent experiments from many machines (FTU, JET, C_MOD) LHCD effects at high plasma density are either completely absent or less than expected. It has been shown, both in FTU and C_MOD, that NRCA of LH wave power can be responsible for that. Indeed NRCA is estimated to be small in JET plasmas, at least in the main heating phase and therefore it is not responsible for the lack of penetration of LHW in high density JET plasmas, however here we show for the first time that it can be effective during the early phase of the current ramp up, when the plasma is still collisional. On the contrary it is suggested that the reduction of LHCD effects at high density may be attributed at least partially to the loss of accessibility of the $n_{||}$ spectrum effectively launched into the plasma.

Current diffusion during the current ramp up has already been analyzed in JET but mainly in discharges without LHCD. Here the current diffusion during the LHCD assisted current ramp up is investigated and a careful comparison between the simulated q profiles and the measured ones is performed over time. The implications of the observed difference are discussed.

Finally the important question of the alignment of all the current profile components is analyzed in JET SS discharges at high β_N, providing useful information if the steady state is achieved in these shots and how far the plasma is from SS.

1. INTRODUCTION

Lower Hybrid Current Drive (LHCD) has been largely used in JET either in the current rump up phase to impact the q profile [1] or in the main heating phase to study the LHCD role in conjunction with bootstrap current and other current driven source terms [2]. In this paper we report on simulations of LHCD in JET high β_N, high-density discharges, both during the LHCD assisted current ramp up and the main heating phase. Important questions to be clarified, strictly related to those experimental scenarios, are: the alignment of the current profile components in high β_N Steady State (SS) JET scenarios [3], and the study of the current diffusion during the current ramp up. Both these issues deserve a deep investigation, since the first was simulated a few times [4] and the second was analyzed in JET [5] but mainly without LHCD (only a limited example exists reported in ref. [6]).

Furthermore, as observed in many experiments [7, 8, 9], JET included [10, 11], LHCD effects

at high plasma density are either completely absent or less than expected. Both in FTU [12] and C_MOD [8, 9] it was shown that Non Resonant Collisional Absorption (NRCA) of LH wave could be responsible for such a phenomenon. Other mechanisms have been proposed as well [7, 10, 13] based on non-linear parametric instabilities [7, 10, 14]. However while these latters were already estimated for JET [10], NRCA of LH waves has never been calculated in JET plasmas and even though it is estimated to be small in the main heating phase, it is important to understand whether it plays a role and in which conditions.

In this paper we face all these original issues: i) analysis of LH-NRCA in JET plasma during the current ramp up phase and in steady state scenarios assessing when it is effective, ii) lack of penetration of LHCD power into high density plasmas iii) study of current diffusion during the LHCD assisted current ramp up and iv) assessment of the current profile alignment in JET Steady State (SS) discharges in the presence of LHCD.

To those aims the relevant JET discharges are simulated all over the discharge duration by ASTRA [15]. The simulation results are closely compared to the available experimental data (such as internal inductance l_i, loop voltage V_{LOOP}, ECE emission, q-profile evolution in time). As a byproduct of this benchmark on JET discharges, and within its limit, we could also deal with a further point: a comparison between LHCD and overshoot technique effects on the q profile in hybrid scenarios [16, 17].

ASTRA is run in the interpretative mode, i.e. taking plasma profiles (like plasma temperatures, density, charge state, Z_{EFF}, and so on) as input data from interpretative TRANSP [18] runs of specific JET discharges. On the contrary the current diffusion equation (Ohm law) is solved in ASTRA taking into account all the Current Driven (CD) current source terms thus allowing the comparison of the simulated q-profile evolution with the experimental. The LHCD current and power deposition profiles are calculated by the FRTC [19,20], a standard Ray tracing Fokker Planck model self-consistently coupled to ASTRA at each temporal step. While a more complete discussion about FRTC is reported in section 3, we remind FRTC includes, besides the quasi-linear electron-damping rate associated to Landau Damping (LD), the *linear damping rate associated to NRCA* [12]. Therefore the ray-power is absorbed or by LD or by NRCA (or by both). Ion Landau damping is also considered in FRTC but it is negligible in the JET experimental condition. As a last possibility, the ray-power can be lost because it is not accessible to the plasma in front of the antenna. This observation, however obvious, is very important as long as you apply it to the $n_{||}$ spectrum *effectively launched into the plasma*. This latter, in fact, may differ from the $n_{||}$ spectrum expected on the basis of the phasing planned a priori (between the multijunction units of the JET antenna [21]). When, on the contrary, the $n_{||}$ spectrum is calculated using the phasing measured a posteriori, it may be distorted and have a low $n_{||}$ part larger than expected. This is shown to happen in shot Pulse No: 72835.

Finally, while in the past LHCD JET discharges have been investigated by ray-tracing Fokker Planck model [22], sometimes coupled to transport code [23], here we analyse several JET discharges following the whole discharge duration and considering all the CD source terms in the Ohm law, thus comparing the simulation results with the available experimental findings.

The paper is organized as follows: in section 2 the most relevant experimental signals of the chosen discharges are presented, in section 3 the main results of the simulations are discussed with the focus on the role of NRCA during the ramp up phase (sec.3.1) and on the fast electron tail reduction at high density (sec.3.2). Section 4 is devoted to the q profile evolution provided by ASTRA and to its comparison to the measured profile, both during the current ramp up and the main heating phase. An assessment of the current profile alignment for JET SS discharges is also provided. Finally the influence on the q profile of LHCD is studied in section 5 and compared to the effect of the current overshoot in section 6. Summary and conclusions follow in section 7.

2. THE EXPERIMENTAL FEATURES OF THE JET PLASMA DISCHARGES

We choose to simulate two experimental scenarios: i) LHCD assisted current ramp up; ii) LHCD during the main heating phase. We simulated two shots of the group i), one quite old (Pulse No: 53430) and one more recent (Pulse No: 77601), and two shots of group ii) (Pulse No: 77893, Pulse No: 72835). All these pulses are from the Carbon Facing Component phase. It is worth reminding that Pulse No: 53430 was part of the ITB program for studying LH coupling in ITB plasma [24], while the shots Pulse No: 77601, Pulse No: 77893 and Pulse No: 72835 are SS scenarios [3] aimed at reaching high β_N (normalized beta) and confinement factor H_{89}.

The Figures 1 and 2 show the experimental signals of the most relevant quantities for these discharges. The box a) shows the plasma current, box b) the Neutral Beam Injected (NBI) power, the Ion Cyclotron Radio Frequency power (ICRF) and LHCD power. Box c) shows the edge and core line integrated electron density. Box d) shows the time trace of D_α displaying when the plasma undergoes the L-H transition. Finally box e) shows the Electron Cyclotron Emission (ECE), at the lowest edge frequency, from fast electrons (at the cyclotron frequency down shifted by relativistic mass effects). While the interpretation of this signal deserves a more accurate analysis, it is recognized that it qualitatively indicates the presence of fast electrons inside the plasma.

We can comment the two shots as follows: Pulse No: 53430 has a slower current ramp (with respect to 77601), higher magnetic field (3.4T against 2.6T) and higher LHCD power in the ramp up phase (2.5MW against 500KW, launched in both discharges at $n_{||} = 1.8$). Plasma density increases after the NBI power switch on (~ 18MW in Pulse No: 53430 and 24MW in Pulse No: 77601) because of the NBI fuelling and of the plasma access to the H mode; the density increase is larger and quite abrupt in 77601, where both the edge and core line averaged density achieve values respectively larger than $0.2\ 10^{20} m^{-2}$ and $1.10^{20} m^{-2}$. In Pulse No: 53430, on the contrary, the line average plasma density core and edge stay below these values. In Pulse No: 77601 the ECE signal, related to the presence of relativistic electrons, drops to zero at t = 4.5s in clear correlation with the plasma density increase. In Pulse No: 53430, conversely, the fast electrons signal starts to increase approximately 1 s after the LH switch on, thus indicating that the electron tail formation into the plasma has a visible delay with respect to the LH switch on.

The Figures 3 and 4 show the experimental signals of the two shots (Pulse No: 77893 and Pulse

No: 72835) belonging to the group ii) (LHCD during the main heating phase). The two shots are similar except for the heating power that is larger in Pulse No: 77893 (24MW of NBI, 6MW of ICRH and 2.5MW of LHCD) than in Pulse No: 72835 (~19MW of NBI, 2.5MW of ICRH and 2.5MW of LHCD). Furthermore the launched LHCD power spectrum is centered at $n_{||} = 2.1$ in Pulse No: 77893 and at $n_{||} = 2.3$ in Pulse No: 72835.

The NBI switch on triggers the H-mode, then the plasma density increases and achieves quite large values both in the core and at the edge, especially in Pulse No: 77893 (where the line average edge and core density reach, even though transiently, 0.4 $10^{20}m^{-2}$ and 1.2810$^{20}m^{-2}$). In correspondence to the density increase the fast electrons signal clearly drops.

3. SIMULATIONS AND MAIN RESULTS

As already mentioned, all the simulations reported hereafter have been performed using the experimental density and temperature profiles provided by TRANSP runs of the considered shots. TRANSP also provides Z_{EFF} (the effective plasma charge state), assumed constant across the radius, and the NBI-CD source. Starting from these input data, ASTRA is run in the interpretative mode, as far as the particle and energy transport equations is concerned, except for the ohm law that is solved, conversely, in the presence of all the sources, i.e. the LHCD source term, calculated by FRTC, the NBI-CD term provided by TRANSP and the Bootstrap Current calculated by NCLASS [25] within ASTRA. In this way simulations provide, besides the LHCD deposition and CD, also the q profiles to be compared to the measured ones.

The plasma equilibrium is calculated in ASTRA by the 3-D momentum solver based on the experimental values of the plasma elongation, triangularity and Shavranov shift. Also the up-down shift of the magnetic axis is considered, while the X point geometry is not included.

The LHCD module, coupled to ASTRA to calculate self-consistently and step by step the LH power deposition and the driven current profile, is a fast ray tracing Fokker Planck model, FRTC [19, 20]. FRTC has been extensively benchmarked on the results of other similar codes [26] and on FTU LHCD driven discharges both in the past [27] and more recently [12].

While a complete discussion about the limit of the linear propagation theory is reported in ref. [12], here we just remind that, as in most the ray tracing codes, also in the FRTC: the $n//$ spectrum is computed along the rays starting from an initial $n//$ spectrum launched near the plasma boundary in the form of the slow mode, the linear mode conversion of the slow wave into the fast wave and back is totally and automatically taken into account along the ray trajectory [28], the ray is specular reflected at the plasma edge cut-off. In short the ray is followed until the transported power is absorbed; only two absorption mechanisms by electrons are considered in the FRTC, the Landau absorption on resonant electrons and the NRCA on thermal electrons, according to the following expression of the power conservation law along the ray:

$$dP_i/d\tau = -2\gamma P_i \,, \qquad (1)$$

where *Pi* is the power assigned to the i^{th} ray and γ is the damping rate. γ consists of two parts $\gamma = \gamma_L + \gamma_C$; γ_L is the quasi-linear damping rate from the Landau resonant wave-electron interaction, and γ_C is the linear non-resonant damping rate due to electron-ion Coulomb collisions (NRCA). γ_C is proportional to the electron ion collision frequency $\nu_{ei} \sim Z_{EFF}\, n_e\, T_e^{3/2}$ (n_e is the plasma density, T_e the electron temperature). NRCA is, therefore, a parasitic power absorption channel for LH waves, occurring in dense cold plasma regions. As shown in ref. [12] NRCA can be a competing absorption mechanism with respect to LD, preventing the electron tail formation and drastically reducing the LHCD efficiency. In ref. [12] NRCA was also suggested to cause the reduction of LHCD efficiency with the electron temperature, reported in all the LHCD experiments.

In addition to being absorbed, a ray may be not accessible to the plasma in front of the antenna: when a ray cannot *be started* at prescribed initial position because there is a no propagation zone, it is discarded from further calculation and its power is lost. Therefore, in FRTC, the ray or it is absorbed by LD and/or by NRCA, or it is lost because it is not accessible.

3.1 THE COLLISIONAL ABSORPTION IN THE VERY EARLY PHASE OF THE CURRENT RAMP UP

In Figure 5 the temporal evolution of the simulated signals provided by ASTRA is reported for Pulse No: 53430: the LH absorbed power, $Q_{LH}(t)$, and the LH driven current, $I_{LH}(t)$. The figure captures a delay of about 1sec between $I_{LH}(t)$ and $Q_{LH}(t)$. There are only two damping mechanisms in FRTC, the Landau Damping (LD) on resonant electrons that generates the fast electron tail and the NRCA occurring at high collisionality. Therefore if the power is absorbed but the current density is not efficiently driven, the only possibility is that the operative damping mechanism is NRCA. Indeed, the initial discharge phase is highly collisional, as shown in Figure 5 where the collisionality $\nu = <\nu_{ei}>/f_{LH}$ (averaged on the plasma volume and normalized to the LH frequency f_{LH}) is plotted. The decrease of ν clearly correlates to the I_{LH} increase. Besides that, the LH power deposition profile ($P_{LH}(\rho)$) and the current density profile ($J_{LH}(\rho)$), shown in Figure 6 at 2 different times (1.5s and 2.0s), have very different shapes ($P_{LH}(\rho)$ is much broader and larger than $J_{LH}(\rho)$ at t = 1.5s than at t = 2.s). The two profiles start to coincide only from the last time, 2s, and keep to be very similar from this time onwards. Also this feature clearly indicates that most of the power is absorbed by NRCA rather than by LD in the initial phase of the current ramp up.

NRCA is present in Pulse No: 77601 current ramp-up too, even though for a short time interval at the beginning of the LH switches on. The g shows the time behavior the different simulated signal (the same as Figure 5) and the Figure 8 shows the $P_{LH}(\rho)$ and $J_{LH}(\rho)$ profiles to have very different shapes at t = 2.3. Conversely, at t = 3s, NRCA is localized mostly at the plasma periphery (Figure 8).

To be more quantitative we report in Figure 9 the percentage of the LH power absorbed by collisions (NRCA) and by LD vs. time, limited to the interval $1 \le t \le 2$s for Pulse No: 53430 and to $2 \le t \le 3$s for Pulse No: 77601. For convenience, the simulated signal $I_{LH}(t)$ is reported as well.

The comparison of these two Figures (9a) and 9b)) shows that in Pulse No: 77601, since from the very beginning, the simulated $I_{LH}(t)$ is not as negligible as in Pulse No: 53430. This is due to the percentage of the power absorbed by LD, which is larger in Pulse No: 77601 in the initial phase, than in Pulse No: 53430. The electron temperature of Pulse No: 53430 is low in the prelude phase and this causes the LD to be very weak even in the central plasma region: this make NRCA the dominant absorption mechanism all over the plasma cross section in the initial phase. The weakness of the LD may the reason why no electron tail is produced just after the LH switch in Pulse No: 53430, as documented by the ECE signal. On the contrary, in Pulse No: 77601, the ECE signal does not display any delay with respect to the LH switch and indeed Figure 9b) is fully compatible with the generation of some electron tail just after the LH switch on. It is clear that is only a reasonable qualitative argument to account for the difference of the ECE signal behavior in Pulse No: 53430 and Pulse No: 77601. A precise statement would require a full ECE signal simulation, which is, however, beyond the scope of this paper.

Another interesting feature occurs in shot Pulse No: 77601, at t = 4.5s: the absorbed power and the driven current both vanish, in spite of the fact that the launched power is still on (see Figure 7). That happens in correspondence of the increase of the plasma density due to H mode and pedestal formation (see Figure 2c). As a matter of fact the launched $n_{||}$ spectrum is not accessible anymore to the plasma at that density and consequently the simulated signals $Q_{LH\_ABS}(t)$ and $I_{LH}(t)$) drop to zero. This drop is in fair good agreement with the ECE signal drop (Figure 2d)) at the same time, indicating a sudden disappearing of fast electrons from the plasma. A further analysis of this issue is postponed to the section 3.2, where it will be dealt together with the same effect occurring in Pulse No: 77893 and Pulse No: 72835.

3.2. LHCD DURING THE MAIN HEATING PHASE AND THE ROLE OF THE ACCESSIBILITY OF THE *EFFECTIVELY LAUNCHED* $n_{||}$ SPECTRUM

The Figure 10 shows the temporal evolution of the simulated signals provided by ASTRA/FRTC for 77893: the LH absorbed power, $Q_{LH\_ABS}(t)$, and the LH driven current, $I_{LH}(t)$, as well as the launched LH power $Q_{LH}(t)$, the total plasma current $I_P(t)$, and the peak density $n_0(t)$. At $t \geq 4.5s$, when the density approaches its maximum value, $Q_{LH\_ABS}(t)$, and $I_{LH}(t)$ both drop to less than half of their previous value, while $Q_{LH}(t)$ is still on at the same power level. As in Pulse No: 77601, this drop is synchronous whith the drop of the ECE signal shown in Figure 3c).

The Figure 11 shows the simulated signals for Pulse No: 72835. Also in this case, at $t \sim 4.3s$, $Q_{LH\_ABS}(t)$, and $I_{LH}(t)$ drop when the edge pedestal density approaches its maximum value. In the interval $3.7s < t \leq 4s$, between the LH power switch on and the sudden increase of the edge pedestal density, ASTRA/FRTC provides a driven current of 160kA, which drops below 100kA later on. In this time interval, where 160kA are driven, a spike is observed in the ECE experimental signal (Figure 4c). The $I_{LH}(t)$ and $Q_{LH\_ABS}(t)$ signals drop again in temporal agreement with the decrease of the ECE signal (Figure 4c).

In all these shots, Pulse No: 77601, Pulse No: 77893, Pulse No: 72835, the drop of the I_{LH} and Q_{LH-ABS} signals, provided by simulations, is strictly related to the density increase that causes, in turn, a lack of accessibility of most or part of the launched power spectrum into the plasma periphery in front of the antenna. As already mentioned, the power in FRTC, or is absorbed by electrons, or it is lost because the starting position of the ray occurs in a non-propagation zone.

As it is well known, LH waves cannot enter as slow waves into a plasma of a given density and magnetic field if $n_{||}$, the local value of the wave refractive index parallel to the magnetic field, is below the local accessible value: $n_{||ACC} \sim 1 + \omega_{pe}/\omega_{ce}$, where ω_{pe} is the electron plasma oscillation frequency and ω_{ce} is the electron cyclotron frequency. Therefore the accessibility condition reads $n_{||} > n_{||ACC}$. The Figure 12 shows the $n_{||}$ spectrum launched into 77601 from the antenna and used in the simulation. The minimum $n_{||}$ can couple to the plasma periphery in front of the antenna, which is located in the Low Field Side, is $n_{||ACC\_LFS} \sim 1 + \omega_{pe}/\omega_{ce}$ calculated at the plasma periphery ($\rho \sim \rho_{PED}$) and in the low field side ($\omega_{ce} = \omega_{ce\text{-}LFS}$), The vertical blue and red lines in Figure 12 highlight $n_{||ACC\_LFS}$ at t = 3s and t = 5s. It moves from 1.5 to 2 showing that the launched spectrum (centered around 1.8) becomes almost wholly inaccessible.

The same occurs in 77893 where a spectrum similar to that reported in Figure 12, but centered at 2.1, was launched by the antenna and used in the simulation. Also this latter becomes partially inaccessible at $t \geq 4.6$. The Figure 13 shows the LHCD current density profiles, J_{LH}, at t = 4s and t = 5.2s. According to the temporal behavior $I_{LH}(t)$ reported in Figure 10, J_{LH} is much smaller at t = 5.2s than at t = 4s.

While Pulse No: 77601 and Pulse No: 77893 are analyzed in this paper for the first time, Pulse No: 72835 is one of the JET discharges at high density where LHCD effects into the plasma are less than expected. For this reason this shot has already been analyzed in previous publications: in ref. [10] PDI, occurring at the plasma edge, are invoked as the dissipation mechanism that prevents the LH power from entering into the plasma. In ref. [22] the accessibility of the $n_{||}$-spectrum, peaked at 2.3, is analyzed for this shot. In particular the Figure 13 of ref. [22] shows $n_{||ACC}$ to stay below $n_{||peak} = 2.3$ over the entire radial profile at a given time. The conclusion was that the accessibility condition does not play a key role in preventing LH penetration in this shot and in general in the puzzling shots at high density. Even though we find here the same result, we come just to the opposite conclusion for the reason reported hereafter: the simulated $I_{LH}(t)$ (Figure 10)) decreases to 1/2 of its value in the time interval t = 4 to t = 4.4, just because the low $n_{||}$ part of the spectrum, effectively launched into the plasma, becomes not accessible. Starting from the *measured* phasing between the 8 multi-junction units of the JET antenna, we calculated, by the ALOHA code [29], the $n_{||}$ spectrum effectively launched into the plasma (Figure 14) (we used it in the simulation). Thus we realized that the antenna launched a distorted $n_{||}$ spectrum into the plasma with only 46% of power in the main peak (at $n_{||} = 2.3$) and almost 10% of the power in the low $n_{||}$ peak (at $n_{||} = 1.7$). The remaining 34% of the power was launched at $n_{||} < 0$ (and since negative $n_{||}$ are not considered in the simulation, this power was disregarded). Therefore, even if $n_{||peak} = 2.3$ is accessible as correctly

reported in ref. [22], nevertheless the accessibility condition plays an important role in this shot because of the spectrum distortion toward lower $n_{||}$. That is clearly illustrated in Figure 14, where the red vertical line corresponds to $n_{||ACC\_LFS}$, the minimum $n_{||}$ value able to couple at the starting position in front of the antenna, at $t \geq 4s$. Similarly the Figure 15 shows $n_{||ACC\_LFS}$ vs. time. The horizontal lines in the Figure highlight the two peaks values $n_{||} = 2.3$ and $n_{||} = 1.7$ of the spectrum: the main peak (2.3) is able to couple to the plasma for the whole duration of the pulse, while the low $n_{||}$ peak (1.7) becomes unable to couple to the plasma at $t > 3.8$- 4s when it gets smaller than the edge $n_{||ACC\_LFS}$ value. All the power in the low $n_{||}$ peak is lost and this causes the decrease of the LH driven current to half of its value. Even though the power loss is only about 10%–20%, the current loss is 50% likely because the fastest wave velocities are missed. The Figure 16 shows the J_{LH} profiles at t = 4s and 4.4s qualitatively indicating a deep decrease of LHCD effects.

We can conclude that in all the cases analyzed here the linear propagation model provides, by the very basic accessibility condition, a robust explanation of the strong attenuation of the electron tail experimentally documented by the ECE signals. Contrary to what reported in ref. [22] the accessibility plays a role also in the case of Pulse No: 72835, one of the shot where LHCD effects at high density are considered (puzzling) less than expected. Indeed 50% of the LHCD drop can be explained by the violation of the accessibility condition, as long as you are using the $n_{||}$ spectrum effectively launched into the plasma. Of course this observation does not preclude other mechanisms to play a role as well.

4. Q PROFILE EVOLUTION AND COMPARISON WITH EXPERIMENTS IN SS SCENARIOS

To look at the q profile evolution, we analyze the shots Pulse No: 77601, Pulse No: 77893 and Pulse No: 72835, starting from the current ramp up phase in Pulse No: 77601. As already mentioned all these discharges are part of the SS scenarios program aimed at reaching high β_N and confinement factor H_{89}. Therefore, since all the current sources are considered in the calculation, namely J_{BS}, J_{LH}, J_{NBI}, their alignment is analyzed, providing information if the steady state is achieved in these shots and/or how far is the current profile from steady state.

ASTRA simulation started at the time where the first experimental q profile was available (by MSE [30] measurement or by polarimetry measurements [31]) as initial condition for the solution of the Ohm's equation.

Besides the current components (Figure 17a)), the Figure 17 shows the temporal traces of several quantities calculated by ASTRA and compared to the corresponding experimental signals (Pulse No: 77601): the loop voltage V_{LOOP} (Figure 17b)), the internal inductance l_i (Figure 17c)), and the central value of the safety factor q, q_0 (Figure 17d)). There is a general good agreement between the calculated and the measured quantity except for q_0 in the ramp up phase, till $t \sim 5s$, when the current ramp up phase and the overshoot phase are completed and the flat top phase starts (see Figure 17a)). During the current ramp up phase, indeed, the q profile evolves faster in simulation

than in measurements. This is well shown in Figure 18: the q profiles, simulated and measured, are displayed at the initial time t = 2.12s, where they are taken equal, and at t = 2.5s (Figure 18a), t = 3s (18b), t = 3.7s (18c) and at t = 6s (Figure 18b). There is a remarkable systematic difference in the simulated and measured q-profile already 0.3s after the start. A faster inward current diffusion, as compared to measurements, was already obtained in simulations of JET Ohmic, NBI and ICRH assisted current ramp up, discharges when a flat Z_{EFF} profile consistent with the line averaged bremsstrahlung measurements was assumed [5]. Also in the present simulations a flat Z_{EFF} profile consistent with measurements is assumed.

In the present calculation of LHCD assisted ramp up, we could use a simple mean to recover a better agreement with the experimental q profile by enhancing, for example, the calculated LH driven current artificially by a given factor, but taking the deposition profile as it is. However, even using a factor 2 in the LHCD efficiency, we could not recover a much more satisfactory result.

From the previous analysis we might infer that neoclassical current diffusion is faster than measured, during the current ramp up. Of course to be convinced we would need errors bars on the measured q-profile that, on the contrary, are not available. The only observation playing in favor of this deduction is the fact that simulated q-profile is systematically lower than the measured one on the whole radial profile and during all the ramp-up phase, as shown in Figure 18. However it is important to note that a peaked Z_{EFF} profile could provide a slower neoclassical current diffusion toward the plasma center yielding a better agreement between measurements and neoclassical simulation results [5].

Bearing in mind the difference found during the ramp-up between the neoclassical current diffusion and the measured one, now we focus (Figure 19) on the simulations results of 77601. The Figure 19a) shows the penetration of the current profile during the ramp up phase until t = 3.7s. Also the LH current profile is shown at t = 3s. It is centered at mid radius and aligned with the bump in the J profile. The corresponding q profiles are shown in Figure 19b). They are very flat in a wide region at $\rho \leq 0.7$. Evolution of current density and q-profile during the main heating phase is shown in Figure 19c)) and d) starting from t = 4s (where NBI and ICRH start, while at t = 4.5s LHCD stops its effects due to inaccessibility) to t = 10s. The current penetration continues from 4s to 6s and after that the current profile tends to peak more and more as shown at t = 10s. At t = 4s the contribution of the bootstrap current is still minor, but when the H mode is well established the bootstrap current become clearly visible in the current pedestal (Figure 19c)). At t = 6s the non-inductively driven current (I_{BS} = 0.6MA, I_{NBI} = 0.27MA) is about 50% of the total current (I_P = 1.756MA) (Figure 17a)). Accordingly the loop voltage, after a transient negative phase ending at t ~ 5s, slightly increases from this time onwards up to 0.1Volts, accounting for the slight decrease of I_{BS}.

During the current flat top, conversely, simulated and measured q profiles are in better agreement, as results from the analysis of Pulse No: 77893 and Pulse No: 72835 reported hereafter. The figures10 and 11 summarized the main signals of the simulation of the two shots Pulse No: 77893 and Pulse

No: 72835. The simulation of Pulse No: 72835 starts at t = 3.7 sec, just before the LHCD and NBI switch on.

In Figure 20a) we report the current components; in 20b) the ASTRA internal inductance is compared to the experimental one, in Figure 20c) the loop voltage and q_0 are compared to the corresponding measured values. The non-inductively driven current, $I_{CD} = I_{BS} + I_{NB} + I_{LH}$, reaches 0.95MA (54% of the total current) at t ~ 5.2s, then the BS component decreases slowly, while V_{LOOP} and l_i correspondingly increase. In the initial phase the experimental q_0 is higher than the calculated, while a good agreement is recovered in the final phase. The vertical lines in Figure 20 b) show the times chosen to compare the q profiles. The Figure 21 shows the measured and simulated q profiles at t = 4, 6.1, 7.2 and 8.9 s. At t = 4s (Figure 21a) the agreement is quite good. In Figure 21 also the total plasma current density profile is shown as well as the other current density components (namely J_{NBI}, J_{BS}, J_{LH}). At t = 6.1s (Figure 21b)) the bootstrap current component is increased, the LHCD component is decreased, and the NBI component is stationary.

The simulation of 77893 starts at t = 3 sec. The initial q profile is chosen equal to the q profile taken from the unconstrained EFIT equilibrium. Again the non-inductively driven current, shown in Figure 22a) with the other components, is 54% of the total current. In the Figure 22b) the simulated loop voltage and q_0 are compared to the corresponding measured values (MSE for q_0). In the initial phase the experimental q_0 is higher than the calculated one. While, in this initial, overshoot phase, the discrepancy is large, a better agreement is recovered in the final phase. The vertical lines in Figure 22 b) show the times chosen to compare the q profiles. The Figure 23 shows the measured and simulated q profiles at t = 4, 6.3s and 10.2s, as well as the total plasma current density and the other current density components. At t = 6.3s (Figure 23b)) the simulated q profile appears larger than the measured profile, because of the large contribution of the bootstrap current at the pedestal location and of the LH current at $\rho = 0.6$. In the final stage, at t = 10.2s, when the total CD contribution has already decreased to almost half of its previous value (Figure 22a)), the q profiles appear in a quite good agreement. The bootstrap peripheral contribution is now much smaller (Figure 23c)) and the total current profile, sustained by the ohmic contribution (V_{LOOP} is increasing in this phase, Figure 22b)), correspondingly shows a current penetration from the outside (to compensate the bootstrap peripheral decrease) and a major peaking in the center. As a side note, observe that the LHCD profile, shown in Figure 23 for 77893 is very similar to that one calculated by CRONOS [32] for a very similar discharge, 77895, as reported in [4].

The SS was not achieved in these shots. Here we added the information that the bootstrap and the other current components contribute to give ~ 50% of non-inductive current. In addition we could look at radial profiles of the current components during the main heating phase (Figure 21b) and 23b)). The alignment looks quite balanced, in view of a SS, since the bootstrap current is broad, from the pedestal to the plasma center, the LHCD current is off axis and the NBI current is peaked.

5. EFFECTS OF LHCD ON THE Q PROFILE

To investigate better the effect of LHCD on the q profile, we consider two more simulations of Pulse No: 77601, one without any LHCD power and the other doubling artificially the LH current drive efficiency, η_{LH}. This affects the q profile evolution and, through it, also the current deposition. All the other parameters of the discharge are taken equal (time and profiles) to the nominal values of the discharge. The Figures 24a) and b) show the comparison of the q profiles at t = 3s, and t = 3.7s for the 3 cases: $J_{LH} = 0$, $\eta_{LH} = \eta_{LH\_FRTC}$, $\eta_{LH} = 2\,\eta_{LH\_FRTC}$. The subsequent time, t = 6s, is not shown, because the LH power does not access anymore from t > 4.5 and, therefore, cannot affect the q profile later on. The Figure 24c) and d) show the corresponding profiles of the total plasma current as it penetrates into the plasma. From these figures we clearly see that LHCD prevents the Ohmic current diffusion toward the plasma center, (limited to the current percentage that, being guided by LHCD, has not to be provided by the transformer) and, as expected, the larger is the percentage of the off axis non inductive current, the larger is the effect. It also allows achieving a flat q-profile at the end of the current ramp up.

6. LHCD FOR HYBRID SCENARIOS

To get hybrid scenario [16, 17] with flat and broaden q profile it is often used the current overshoot technique [33] properly timed with the main heating phase to freeze the q profile later on. Some overshoot is attempted also in Pulse No: 77601 but it is somewhat negligible (even though Pulse No: 77601 belongs to SS scenarios and not to hybrid scenarios). In ITER this technique might not be used because of flux consumption [34], therefore it would be desirable to have other means to prepare and keep the hybrid q profile using, for example, off axis current drive, as LHCD can provide. We try here to compare the effect, on the q-profile, of the current overshoot and of the LHCD only. To this aim we consider two more simulations. As in the previous case we used all the parameters of the shot Pulse No: 77601 (density temperature, NBI, etc.), only changing the temporal behavior of the total plasma current for a small time interval, as shown in Figure 25a): to make the overshoot effect more visible we added some extra current in the overshoot phase (up to 2MA). Furthermore in the simulation with LHCD and without the overshoot, the LHCD power has the same wave-form as in Pulse No: 77601, but is launched at higher $n_{||}$, $n_{||} = 2.1$, to avoid the lack of accessibility at t = 4.5 and allow the power to enter into the plasma also in the main heating phase. That is shown in the Figure 25b) where the absorbed LHCD power and the driven current are displayed. The use of the same pressure profiles (as well as current density sources, namely J_{NBI} and J_{BS}) in the two simulations makes the calculation only indicative and deserves some comment. The effects on plasma temperature of a larger current overshoot (300kA instead of 150kA) in one case, and of a larger LHCD power (2MW) entering into the plasma at t > 4.5s in the LHCD case, are not taken into account, while they can be different. A larger LHCD power should increase the average electron temperature $\Delta T_E / T_E$ at t > 4.5s by a percentage proportional to $1/2\ \Delta P/P_{TOT} = 2MW/25MW \sim 4\%$ through its effect on confinement. Such a small effect is not able to change the LHCD profile. By

the same reason the transient effect of the overshoot on the averaged electron temperature would be proportional to $0.9\ \Delta I_P/I_P \sim 6\%$ in the time interval $3.5s < t < 5s$. Regardless if those effects are small or not, the aim here is not suggesting a precise experiment, or giving a realistic description of what would be the difference of all the parameters in two realistic discharges. On the contrary we are considering a sort of ideal experiment where the 2 discharges have the same temperature and density profiles but differ in the way to affect the q profile. In principle that is possible, by varying, for example, some additional heating power (like ICRF) without affecting the current drive. Furthermore, just because the pressure profile is kept equal, the equilibrium of the two cases will be different to account for the different current profile.

The results of the overshoot/LHCD comparison are summarized in Figure 25a) displaying the time evolution of q_0 in the two cases: q_0 is higher in the LHCD case, since, as already noted, LHCD subtract current from the plasma center driving it off axis and making the current density profile broader. That is clearly displayed in Figure 26a) and b) where the J and q profiles for the LHCD and the overshoot case are compared just at the end of the overshoot ($t = 5.5s$) phase and later on, at $t = 6.8s$. The internal inductance results higher for the overshoot case. The difference in the shear $\Delta s = (s_{OV} - s_{LH})$ is shown in Figure 27: at $t = 5.5s$ the difference is very small at $\rho < 0.6$ and grows in the interval $0.6 < \rho < 0.9$; at $t = 56.8s$ the difference is negligible at $\rho < 0.5$ and grows at $\rho > 0.5$.

On the basis of these results we can conclude that LHCD, at a few MW level, affects the q profile likewise the current overshoot, with the advantage of producing a flatter and higher q-profile in the plasma center ($\rho < 0.5$). At the LHCD power level considered here (that is a realistic power level for the JET LHCD system) also the stability of the hybrid scenario is similar, since the Ohmic current, that is an important fraction of the total current, dominates the q profile time evolution leading to a progressive peaking of the current profile in both cases. Such a peaking is however less in the LHCD case. Of course to have a major benefit on the stability one would need more LHCD power.

SUMMARY AND CONCLUSIONS

We have simulated 4 JET discharges in the presence of LHCD by means of ASTRA/FRTC, in order to investigate some main issues within the limit of the LHCD linear propagation model: i) analysis of Non Resonant Collisional Absorption (NRCA) of LH wave power at JET during the current ramp up phase and in steady state scenarios, ii) lack of LH power penetration in high density plasmas, iii) current diffusion during the LHCD assisted current ramp up, iv) assessment of the current profile alignment in JET Steady State (SS) discharges in the presence of LHCD. To this aim we have compared in detail the simulation results with the available relevant experimental signals. The main results and novelties of this analysis can be summarized as follows:

- The Non Resonant Collisional Absorption (NRCA) of LH waves is shown for the first time to be operative in two JET simulations at the beginning of the current ramp up phase when the plasma collisionality is still high. In particular NRCA accounts for the temporal delay of the LH driven current with respect to the launched power. This delay is experimentally documented,

even though only qualitative, by the temporal behavior of ECE emission at the Down Shifted frequency.

- Penetration of LH power is lacking in JET high-density plasmas and in some shots, as in Pulse No: 72835, fast electrons are sharply reduced while LHCD is still on. In this paper we show that the simulated LH driven current sharply drops in perfect synchronism with the fast electron ECE signal and that this drop is simply due to the lack of accessibility of the whole or a part of the launched spectrum. In particular, in the case of Pulse No: 72835, that is one of the high density shot considered puzzling when previously analized through the linear propagation model, it was important to regognize that the spectrum launched into the plasma was distorted and had a low $n_{||}$ part larger than expected. This shows that the $n_{||}$ spectra should be calculated, or at least checked time to time, on the basis of the measured phasing between the multijunction units.

- As far as the q profile evolution and its comparison to the experiments, we confirmed that in the current ramp phase there is a systematic difference in the simulated and measured q-profile already quite soon after the start of the simulation: neoclassical current diffusion seems to be faster than measured, during this phase. On the contrary during the current flat top a better agreement is found. This subject, however, deserves more investigation, since the errors bars on measurements can be very large and are not well known indeed. Furthermore a flat Z_{EFF} profile was assumed in the present simulations, while a peaked one is expected to provide a slower neoclassical current diffusion toward the plasma center possible yielding a better agreement between measurements and neoclassical simulation results [5].

- Since we calculated LHCD and all the other current components for the whole duration of the pulse, we were able to provide an assessment of the current profile alignment for JET SS discharges. According to our calculation, a non-inductive current fraction between 49% and 54% was driven during the main heating phase in the three SS considered shots. The current components alignment looked well balanced, in view of a SS, in the main heating phase and the slow increase in time of the experimental V_{LOOP} and l_i signals was well reproduced by the calculation.

- We also highlighted that LHCD prevents, as expected, the Ohmic current diffusion toward the plasma center, and the larger is the percentage of the off axis non inductive current, the larger is this effect. Furthermore we showed that LHCD could replace in JET, at least in principle, the current overshoot technique to prepare the q-profile of Hybrid scenarios. The simulations indicate that LHCD subtract current from the plasma center thus making the current density profile broader.

ACKNOWLEDGEMENT

This work was supported by the EURATOM Communities, under the contract of Association between EURATOM/ENEA. The views and opinions expressed herein do not necessarily reflect those of the European Commission.

REFERENCES

[1]. F. Crisanti et al. Physical Review Letters **88**, 145004 (2002)

[2]. C.D. Challis et al 2001 Plasma Physics and Controlled Fusion **43** 861 doi:10.1088/0741-3335/43/7/303

[3]. J. Mailloux, X. Litaudon, et al, "Towards a Steady-State Scenario with ITER Dimensionless Parameters in JET", 23rd IAEA Fusion Energy Conference, Daejon, Republic of Korea, **10–16** October 2010

[4]. Garcia et al, Nuclear Fusion **51** (2011) 073019

[5]. Voitsekhovitch et al 2010 PPCF **52** 105011

[6]. F. Imbeaux et al 2011 Nuclear Fusion **51** 083026 doi:10.1088/0029–5515/51/8/083026

[7]. R. Cesario et al 2010 Nature Communications; doi: 10.1038/ncomms 1052

[8]. G.M. Wallace et al. 2010 Physics of Plasmas **17** 082508;

[9]. G.M. Wallace et al 2011 Nuclear Fusion **51** 083032 doi:10.1088/0029–5515/51/8/083032

[10]. R. Cesario et al 2011 Plasma Physics and Controlled Fusion **53** 085011 doi:10.1088/0741-3335/53/8/085011

[11]. K. Kirov et al 2010 Nuclear Fusion **50**

[12]. E. Barbato 2011 Nuclear Fusion **51** 103032

[13]. V. Pericoli Ridolfini et al 2011 Nuclear Fusion **51** 113023 doi:10.1088/0029-5515/51/11/113023

[14]. S.G. Baek et al – 2012 – psfc.mit.edu

[15]. Pereverzev G.V. and Yushmanov P.N. 2002 Report IPP 5/98, Max-Planck-Institute fur Plasmaphysik

[16]. Joffrin E. et al 2010 Proc. 23rd Int. Conf. on Fusion Energy 2010 (Daejeon, Republic of Korea) (Vienna: IAEA)CD-ROM file EX/1-1]. and http://wwwpub.iaea.org/mtcd/meetings/PDFplus/2010/cn180/cn180 papers/exc 1-1.pdf

[17]. M.N.A. Beurskens et al 2013 Nuclear Fusion **53** 013001 (17pp) doi:10.1088/00295515/53/1/013001

[18]. Goldston R.J., McCune D.C., Towner H.H., Davis S.L., Hawryluk R.J. and Schmidt G.L. 1981 Journal of Computational Physics **43** 61

[19]. A.R. Esterkin and A.D. Piliya 1996 Nuclear Fusion **38** 1501

[20]. E. Barbato and A. Saveliev 2004 Plasma Physics and Controlled Fusion **46** 1283

[21]. X. Litaudon and D. Moreau 1990 Nuclear Fusion **30** 471 doi:10.1088/0029–5515/30/3/009

[22]. M. Goniche *et al* 2010 Plasma Physics and Controlled Fusion **52** 124031 doi:10.1088/0741-3335/52/12/124031

[23]. T.J.J. Tala et al 2000 Nuclear Fusion **40** 1635 doi: 10.1088/0029–5515/40/9/308

[24]. Mailloux J. et al 2002 Physics of Plasmas **9** 2156-64
[25]. Houlberg W.A., Shaing K.C., Hirshman S.P. and Zarnstorff M.C. 1997 Physics of Plasmas **4** 3230
[26]. C. Gormezano et al 2007 Nuclear Fusion **47** S285 doi: 10.1088/0029–5515/47/6/S06
[27]. E. Barbato et al 2004 Fusion Science and Technology **45** Chapter 3 p. 323
[28]. J.A. Heikkinen, T.J.J. Tala, T.J. H Pättikangas, A.D. Piliya, A.N. Saveliev and S.J. Karttunen 1999 Plasma Physics and Controlled Fusion **41** 1231–1249.
[29]. J. Hillairet et al 2010 Nuclear Fusion **50** 125010 doi: 10.1088/0029–5515/50/12/125010
[30]. N.C. Hawkes et al. 1999 Review of Scientific Instruments **70** 894
[31]. F.P. Orsitto et al 2008 Plasma Physics and Controlled Fusion **50** 115009
[32]. Artaud J.F. et al 2010 Nuclear Fusion **50** 043001
[33]. J. Hobirk et al 2012 Plasma Physics and Controlled Fusion **54** 095001
[34]. Hogeweij et al 2013 Nuclear Fusion **53** 013008

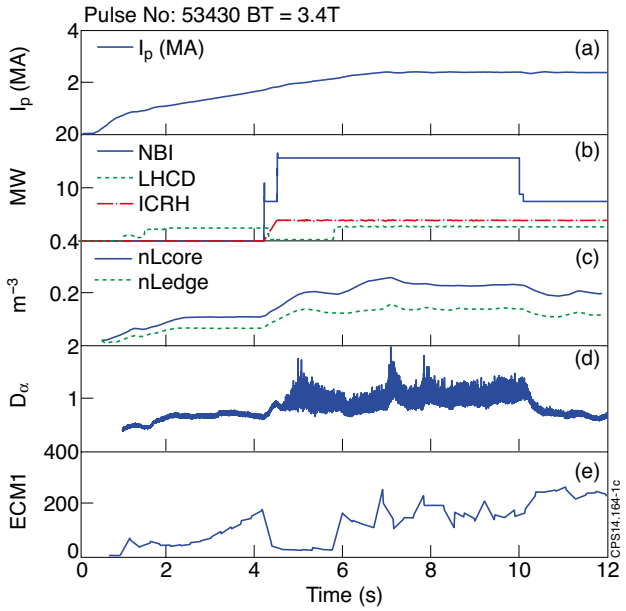

Figure 1: Pulse No: 53430 experimental signals: a) plasma current; b) additional heating power: NBI (blue line), LH (green line), ICRH (red line); c) core (blue) and edge (green) line averaged density; d) D_α signal; e) ECE emission at the lower frequency edge.

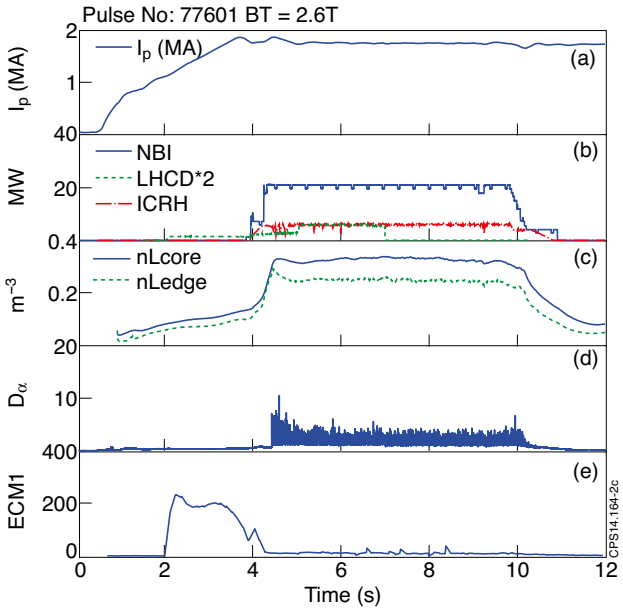

Figure 2: Pulse No: 77601 experimental signals: a) plasma current; b) additional heating power: NBI (blue line), 2 x LH (green line) (to make the signal more visible the LH power signal has been artificially multiplied by a factor 2), ICRH (red line); c) core (blue) and edge (green) line averaged density; d) D_α signal; e) ECE emission at the lower frequency edge.

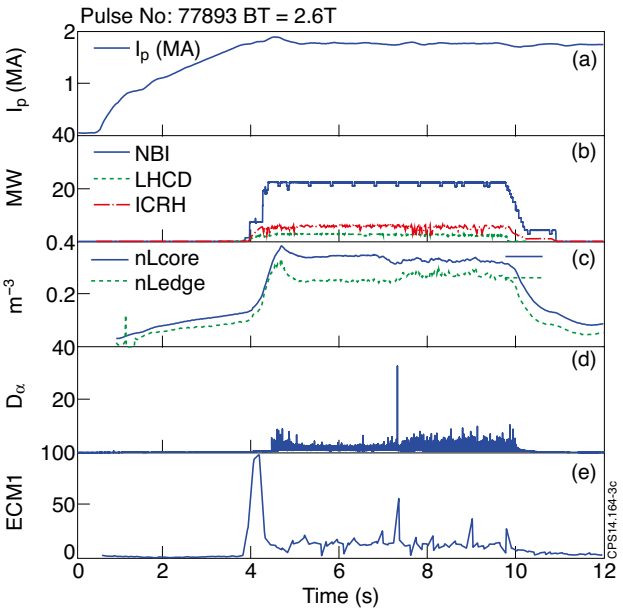

Figure 3: Pulse No: 77893 experimental signals: a) plasma current; b) additional heating power: NBI (blue line), LH (green line), ICRH (red line); c) core (blue) and edge (green) line averaged density; d) D_α signal; e) ECE emission at the lower frequency edge.

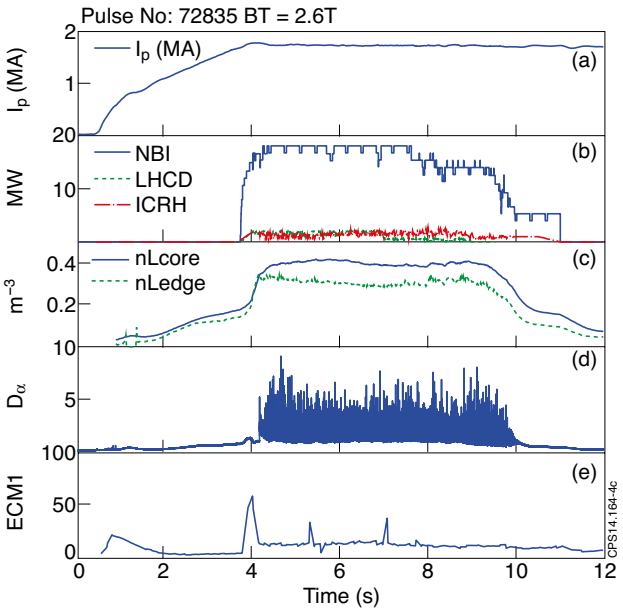

Figure 4: Pulse No: 72835 experimental signals: a) plasma current; b) additional heating power: NBI (blue line), LH (green line), ICRH (red line); c) core (blue) and edge (green) line averaged density; d) D_α signal; e) ECE emission at the lower frequency edge.

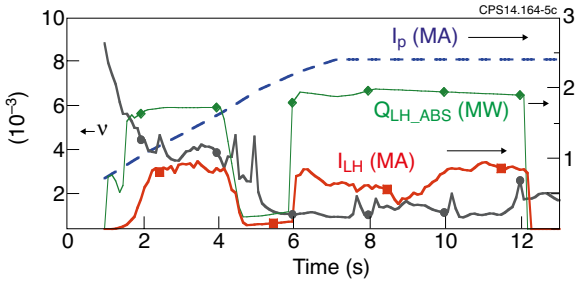

Figure 5: Simulation of Pulse No: 53430: LH absorbed power Q_{LH_ABS} (green diamonds) and LH current driven ILH (red squares). A delay of 1s is visible between the I_{LH} (t) and Q_{LH_ABS} (t) signals. The increase of I_{LH} correlates to the decrease of the collisionality n (black circles) The plasma current is also shown (dashed blue line) to highlight the LHCD contribution in the range 80% ÷ 50% of the total current in the time interval 2s ÷ 4.5s.

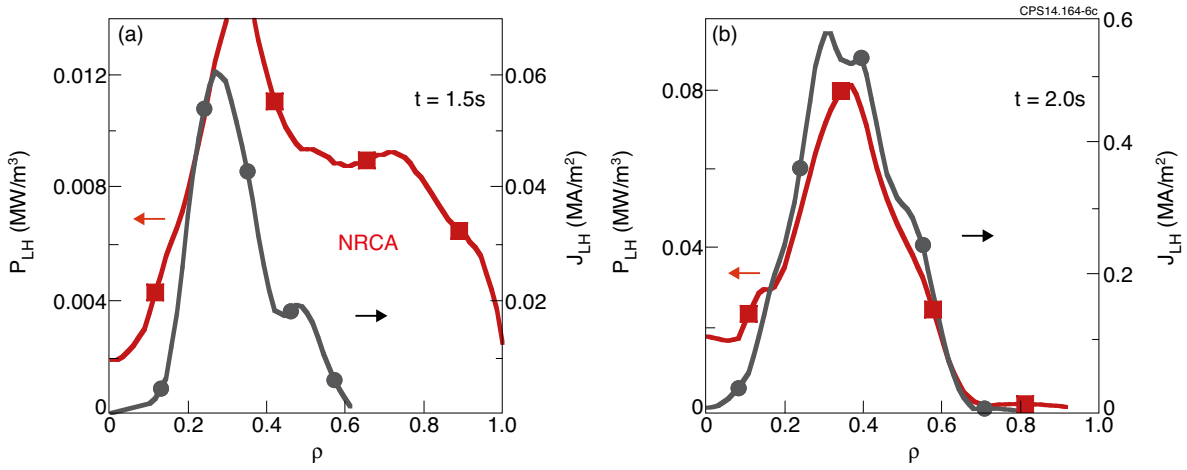

Figure 6: Simulation of Pulse No: 53430: LH power deposition profile (PLH, red squares, left scale) and LH current density profile (J_{LH}, black circles, right scale) at 2 different times, at the beginning of LH current increase (see Figure 5): a) the deposition profile is broader than the current density profile at t < 2s indicating that NRCA is operative at a larger extent with respect to Landau damping; b) starting from t = 2s, NRCA is not operative anymore and the two profiles (P_{LH} and J_{LH}) coincide.

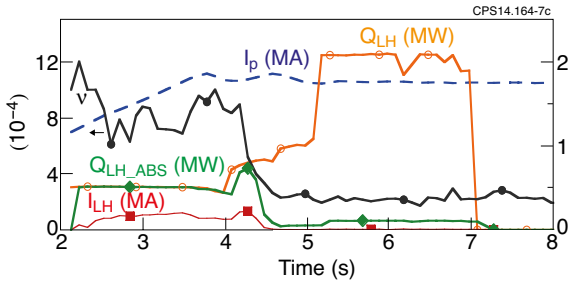

Figure 7: Simulation of Pulse No: 77601: Launched LHCD power (Q_{LH}, orange empty circles, right scale), LH absorbed power Q_{LH_ABS} (green diamonds, right scale) and LH current driven I_{LH} (red full squares, right scale). A delay of about 0.4s is visible between the I_{LH} (t) and Q_{LH} (t) signals. The increase of I_{LH} correlates to the decrease of the collisionality n (black full circles, left scale)

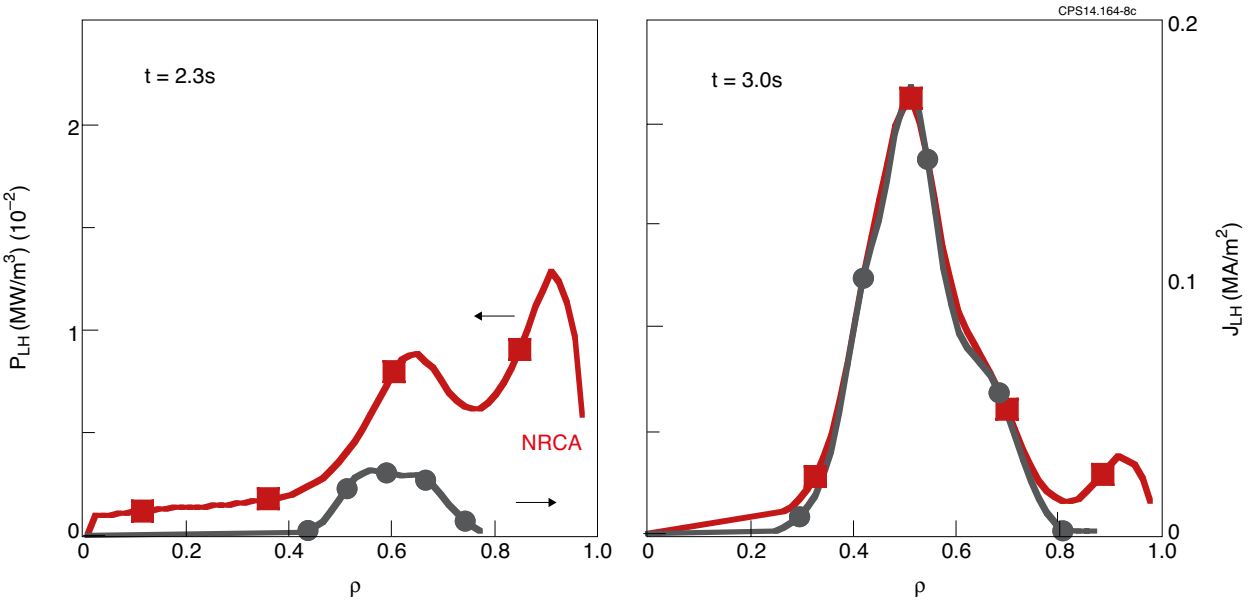

Figure 8: Simulation of Pulse No: 77601: LH power deposition profile (P_{LH}, red squares, left scale) and LH current density profile (J_{LH}, black circles, right scale) at 2 different times. At t = 2.3 the deposition profile is larger than the current density profile indicating that NRCA is operative at a larger extent with respect to Landau damping. At t = 3s NRCA is localized mostly in the plasma periphery. A t > 3.5s is not operative anymore.

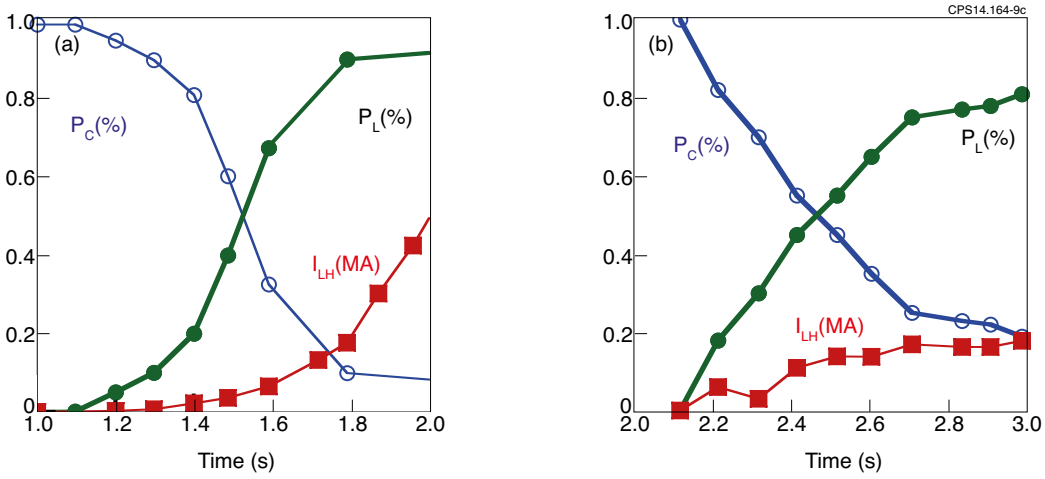

Figure 9: Percentage of power absorbed by NRCA, P_c (blue empty circles), and by LD, P_L (green full circles), vs. t. For convenience also the LH driven current, I_{LH} (red full squares) is shown. Only the early phase of the discharge is reported a) Pulse No: 53430 and b) Pulse No: 77601. NRCA dominates longer in Pulse No: 53430 than in Pulse No: 77601.

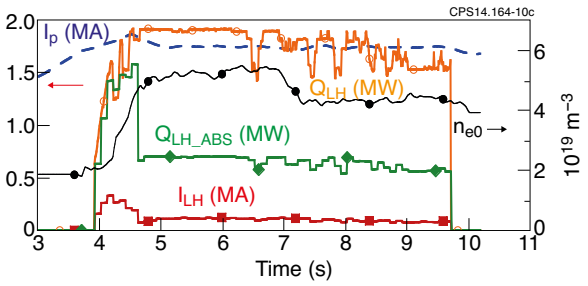

Figure 10: Simulation of Pulse No: 77893: Launched LHCD power (Q_{LH}, orange empty circles, left scale), LH absorbed power Q_{LH_ABS} (green diamonds, left scale) and LH current driven I_{LH} (red full squares, left scale), peak electron density n_{e0} (full circles, right scale). At t = 4.6s Q_{LH_ABS} and I_{LH} both drop, when the plasma density increases toward its maximum value.

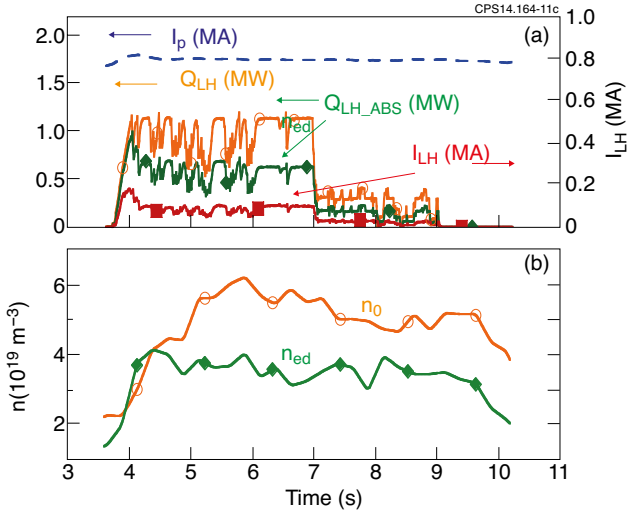

Figure 11: Simulation of Pulse No: 72835: a) Launched LHCD power (Q_{LH}, orange empty circles, left scale), LH absorbed power Q_{LH_ABS} (green diamonds, left scale) and LH current driven I_{LH} (red full squares, right scale), the total plasma current is also shown (blue dashed line, left scale). At t = 4.2 Q_{LH_ABS} and I_{LH} both drop, when the edge plasma density approaches its maximum value, as shown in b). b) Peak electron density n_{e0} (orange open circles) and edge electron density n_{ed} (green diamond). At t = 4.2 (indicated by the vertical dashed line) the edge plasma density approaches its maximum value and Q_{LH_ABS} and I_{LH} both drop.

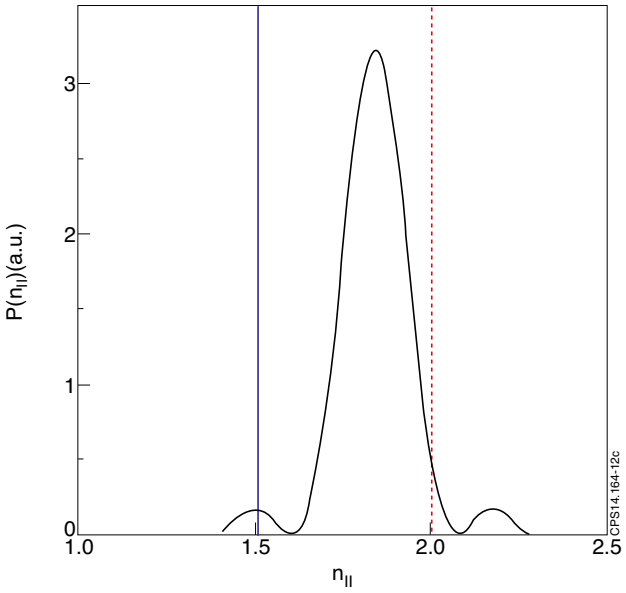

Figure 12: $n_{//}$-power spectrum launched into Pulse No: 77601. The vertical line indicate the $n_{//ACC\_LFS}$ value in the periphery in the LFS at t = 3s (blue continuous line) and at t = 5s (red dashed line).

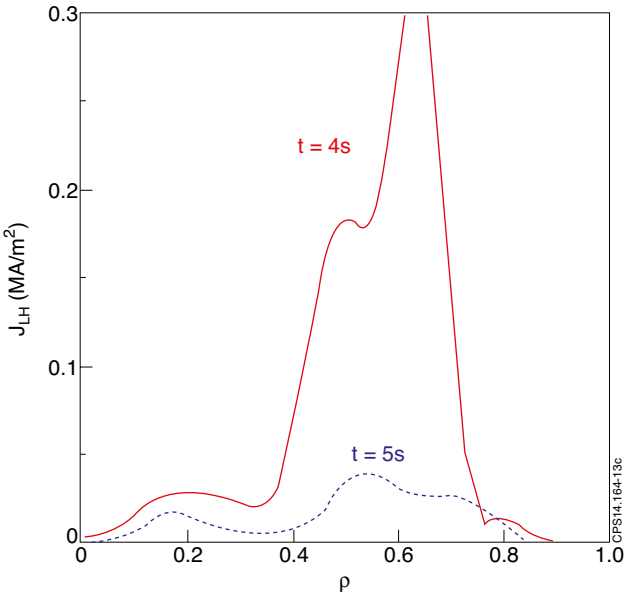

Figure 13: Pulse No: 77893: LH current density profile at t = 4s (red continuous line) and t = 5.2s (blue dashed line) when most of the power spectrum is not accessible to the plasma anymore.

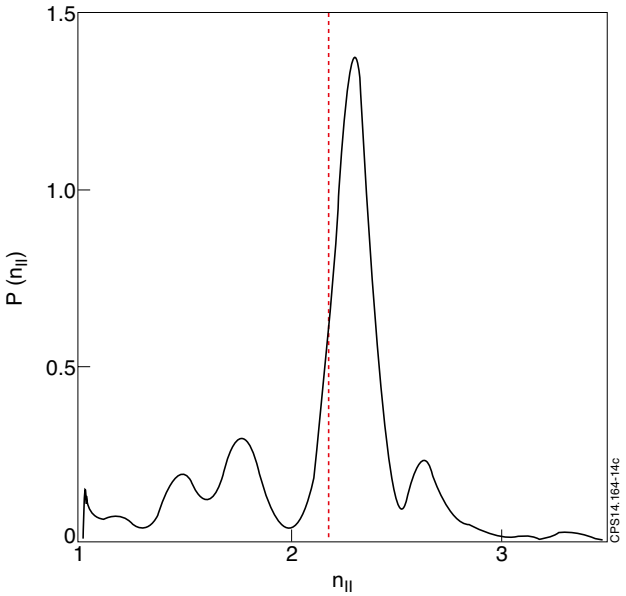

Figure 14: Power spectrum launched in Pulse No: 72835. It is the positive part ($n_{//} > 0$) of the power spectrum calculated by ALOHA [29]. The red vertical line indicates the $n_{// ACC\_LFS}$ value in front of the antenna at $t \geq 4s$.

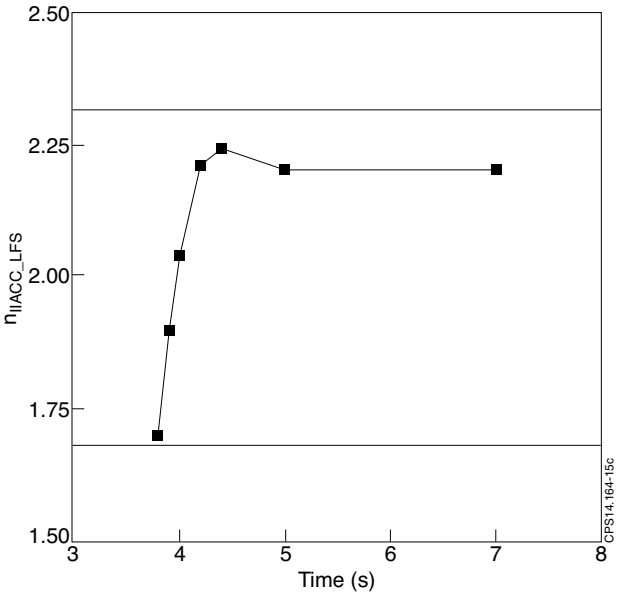

Figure 15: Pulse No: 72835: edge value of $n_{//ACC\_LFS}$, vs. t, rapidly growing above 1.7 between t = 3.8s and t = 4s

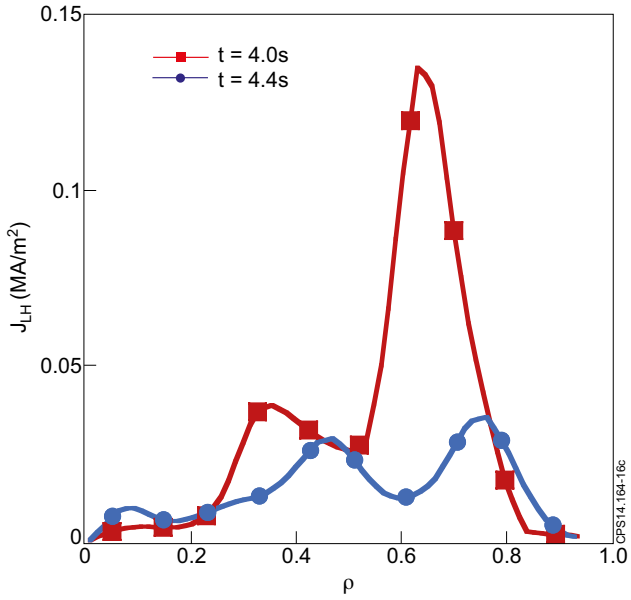

Figure 16: Pulse No: 72835; LH current density profiles at t = 4s (red squares) and t = 4.4s (blue circles).

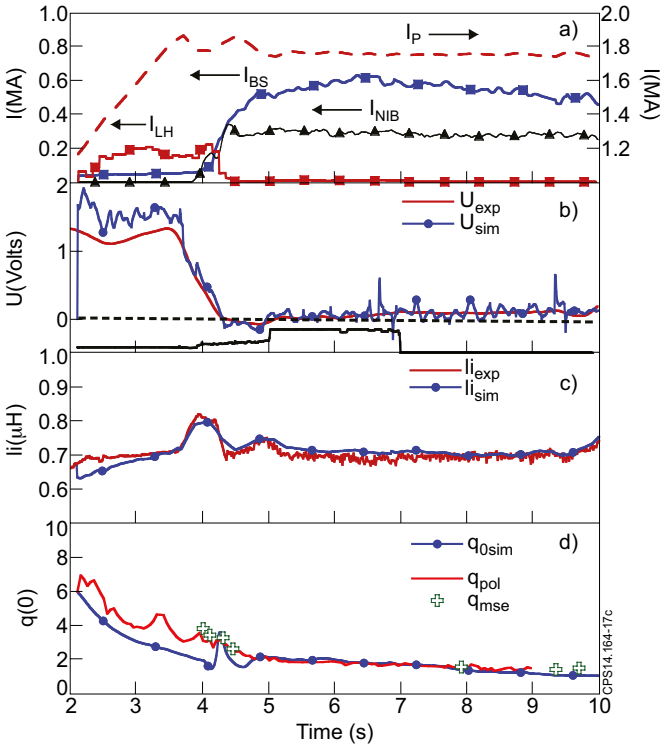

Figure 17: Pulse No: 77601; a) plasma current components, I_P (total current, right scale, red dashed line), I_{BS} (bootstrap current, left scale, blue squares), I_{NB} (NBCD, left scale, black triangles), I_{LH} (LHCD, left scale, red squares); comparison between simulation (blue full circles) and experimental signals (red continuous line) b) loop voltage U, c) internal inductance li, d) central value of the safety factor, q(0) (the experimental red continuous line signal is from polarimetric measurement, q_{pol}, the green crosses are from MSE, q_{mse}).

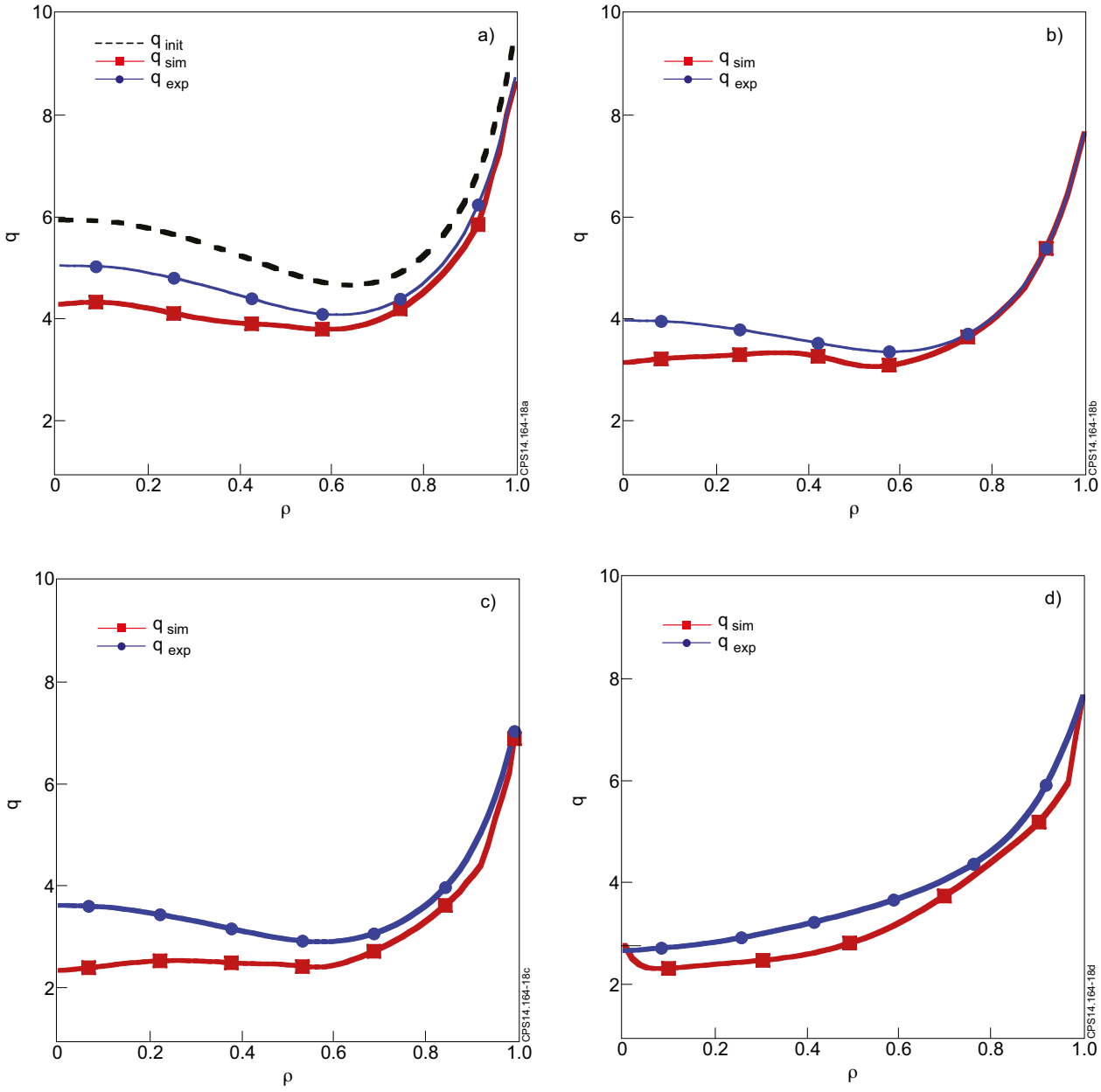

Figure 18: Pulse No: 77601; comparison of simulated (red squares) and measured (blue circles) q profiles: a) at t = 2.5s, b) at t = 3s, c) t = 3.7s and d) at t = 6s. The dashed line in a) is the measured q profile at t = 2.12s, assumed as initial q profile in the simulation.

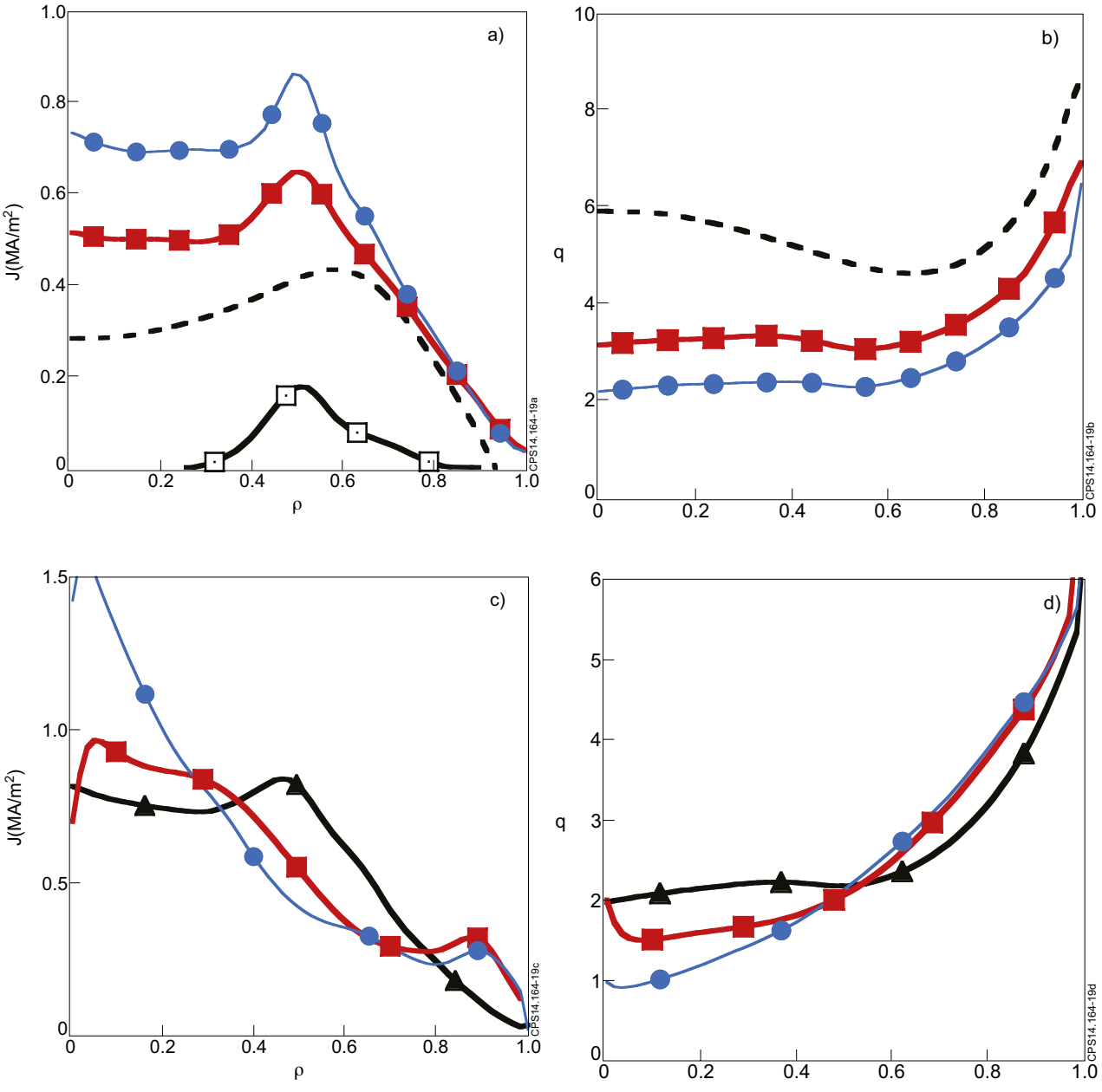

Figure 19: Pulse No: 77601. Temporal evolution of current density and q profiles from ASTRA simulation; a) J profile during the ramp up phase, t = 2.12 (dashed line), t = 3s (red squares), t = 3.7s (blue circles), also the LH current density at t = 3s profile is shown (empty squares); b) corresponding q profile during the ramp up phase (same legend as in a)); c) current penetration and d) q profile evolution during the main heating phase: t = 4s (black triangles), t = 6s (red squares), t = 10s (blue circles).

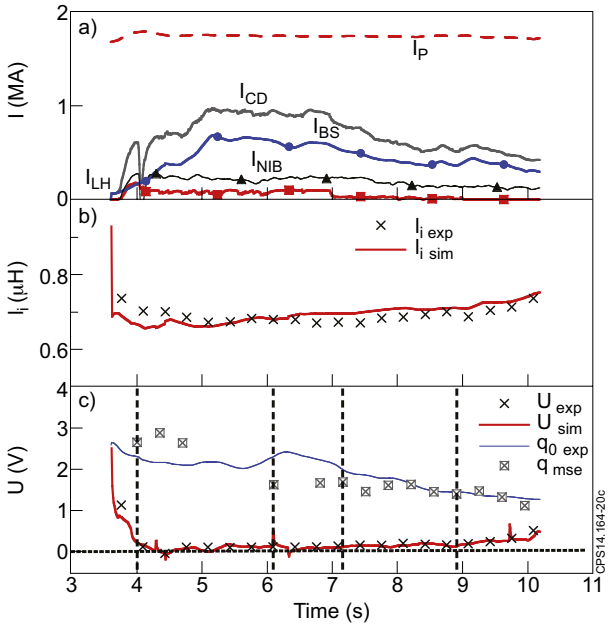

Figure 20: Pulse No: 72835. a) Current components, I_P (total current, red dashed line), I_{BS} (bootstrap current, blue circles), I_{NB} (NBCD, black triangles), I_{LH} (LHCD, red squares), I_{CD} (total driven current, grey continuous line); b) ASTRA internal inductance (red continuous line) compared to the experimental one (black crosses); c) ASTRA loop voltage (red continuous line) and q_0 (blue continuous line) are compared to the corresponding measured values (crosses and squares). The horizontal dashed line highlights the 0 loop voltage level. The vertical lines show the times chosen for the q-profile comparison reported in the next figure.

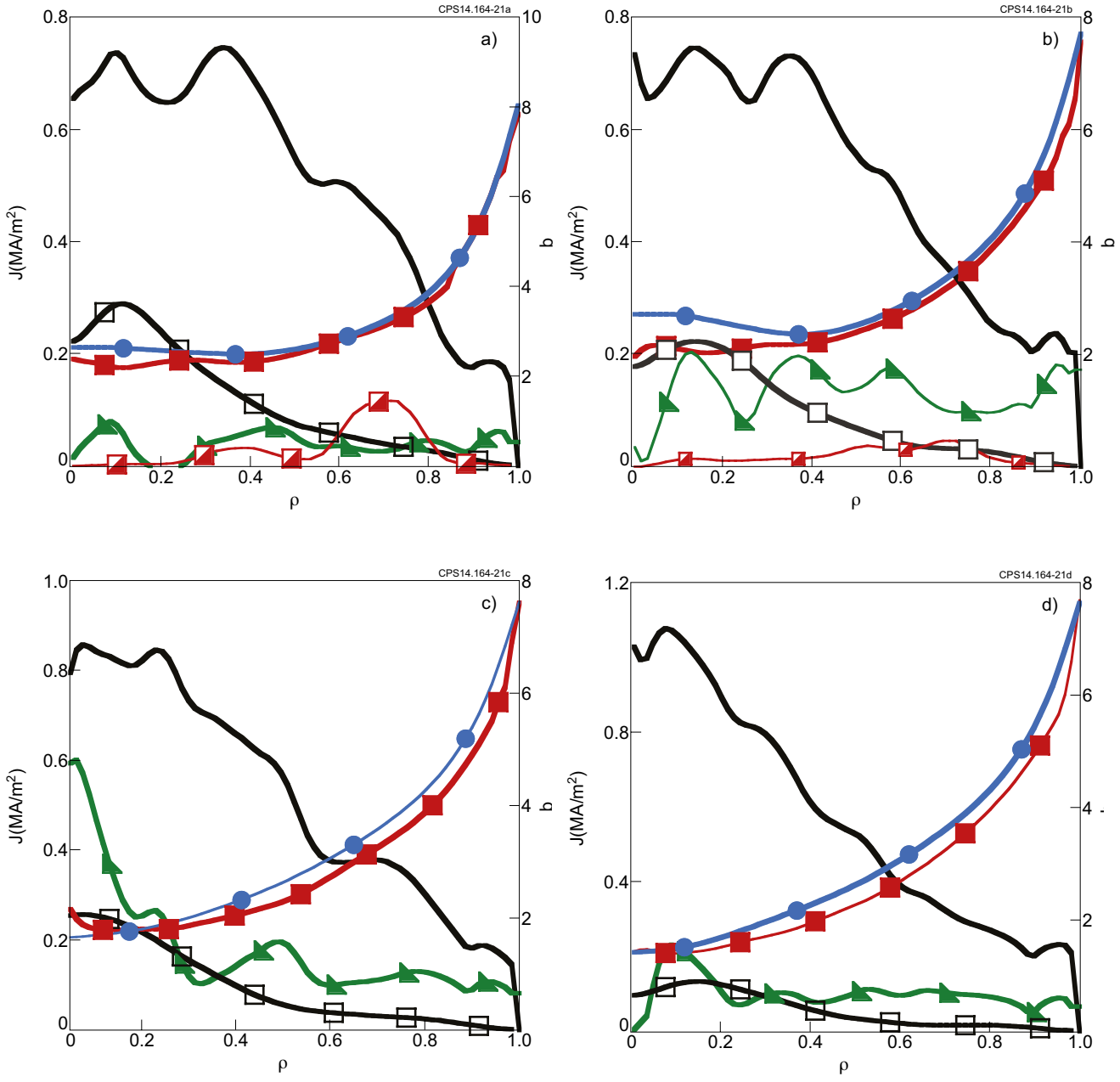

Figure 21: Pulse No: 72835; Comparison of the simulated (red squares) and measured (blue circles) q profile during the main heating phase. a) t = 4s, b) t = 6.1s, c) t = 7.2s, d) t = 8.9 s. In a) all the current density components are shown: J total (black continuous line), J_{NBI} (empty black squares), J_{BS} (green triangles), J_{LH} (red half full squares).

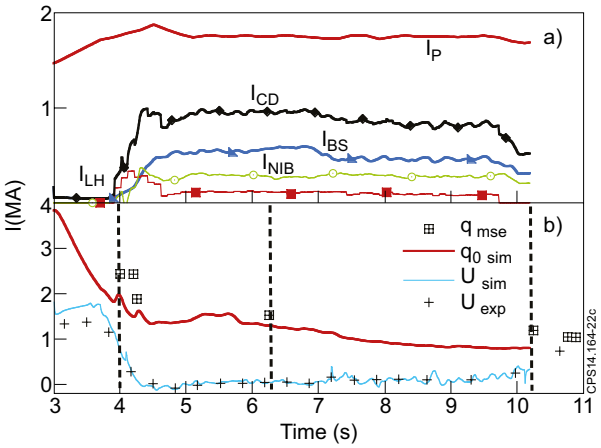

Figure 22: Pulse No: 77893 a) plasma current components, I_P (red line), I_{BS} (light blue triangles), I_{NBI} green open circles), I_{LH} (red squares), total driven current I_{CD} (black diamond); b) simulated loop voltage (light blue line) compared to the experimental loop voltage (black crosses) and simulated q_0 (red line) compared to measured values (MSE) (crossed squares). The vertical lines, in b), indicate the times chosen for the q profile comparison shown in the next figure.

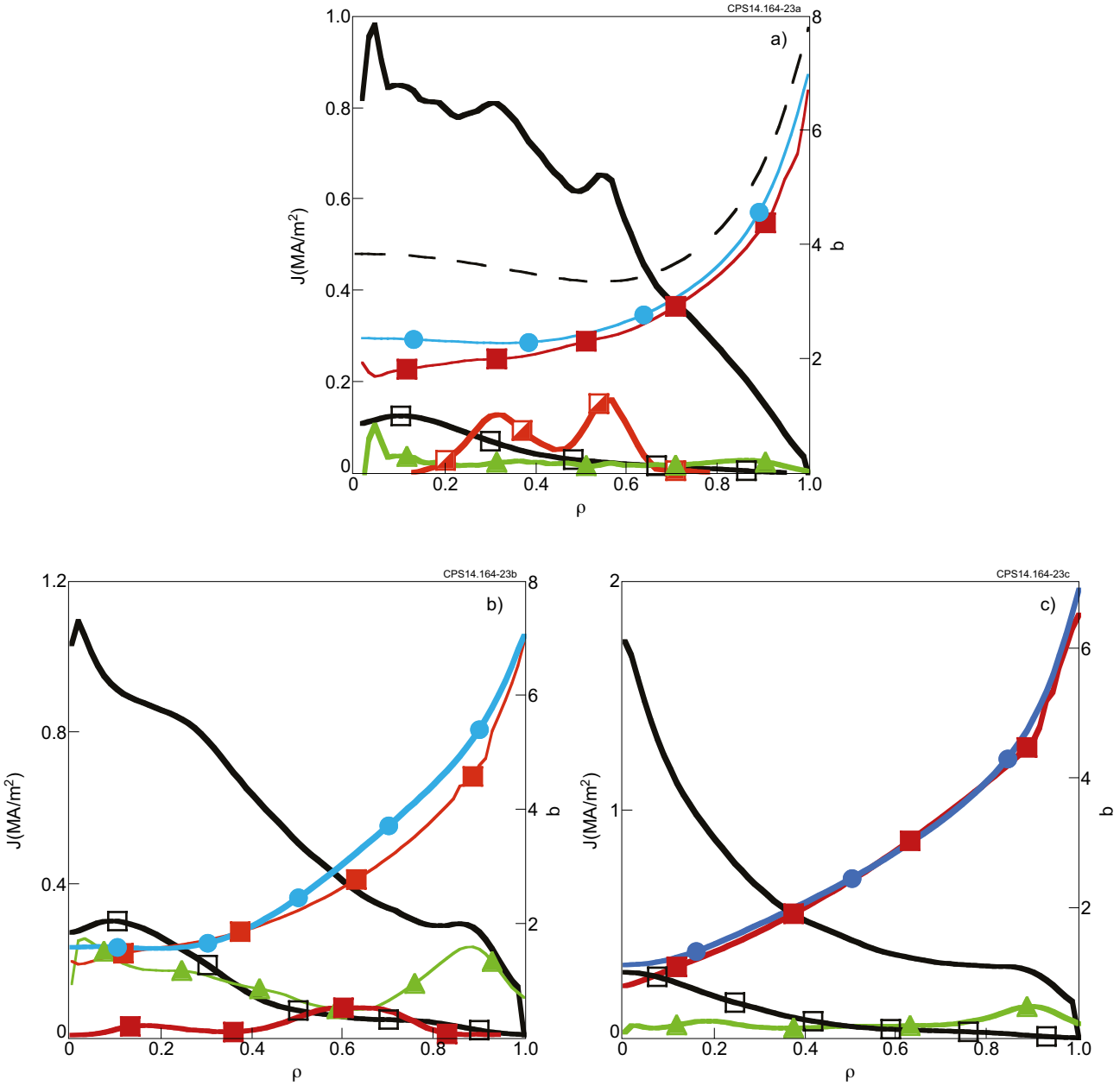

Figure 23: Pulse No: 77893. Comparison of the simulated (red squares) and measured (blue circles) q profiles, during the main heating phase: a) t = 4s, b) t = 6.3s, c) t = 10.2s. In a) also the initial q profile is shown (dashed black line). Also total J (black continuous line), J_{NBI} (empty black squares), J_{LH} (red half-full squares), J_{BS} (green triangles) are shown.

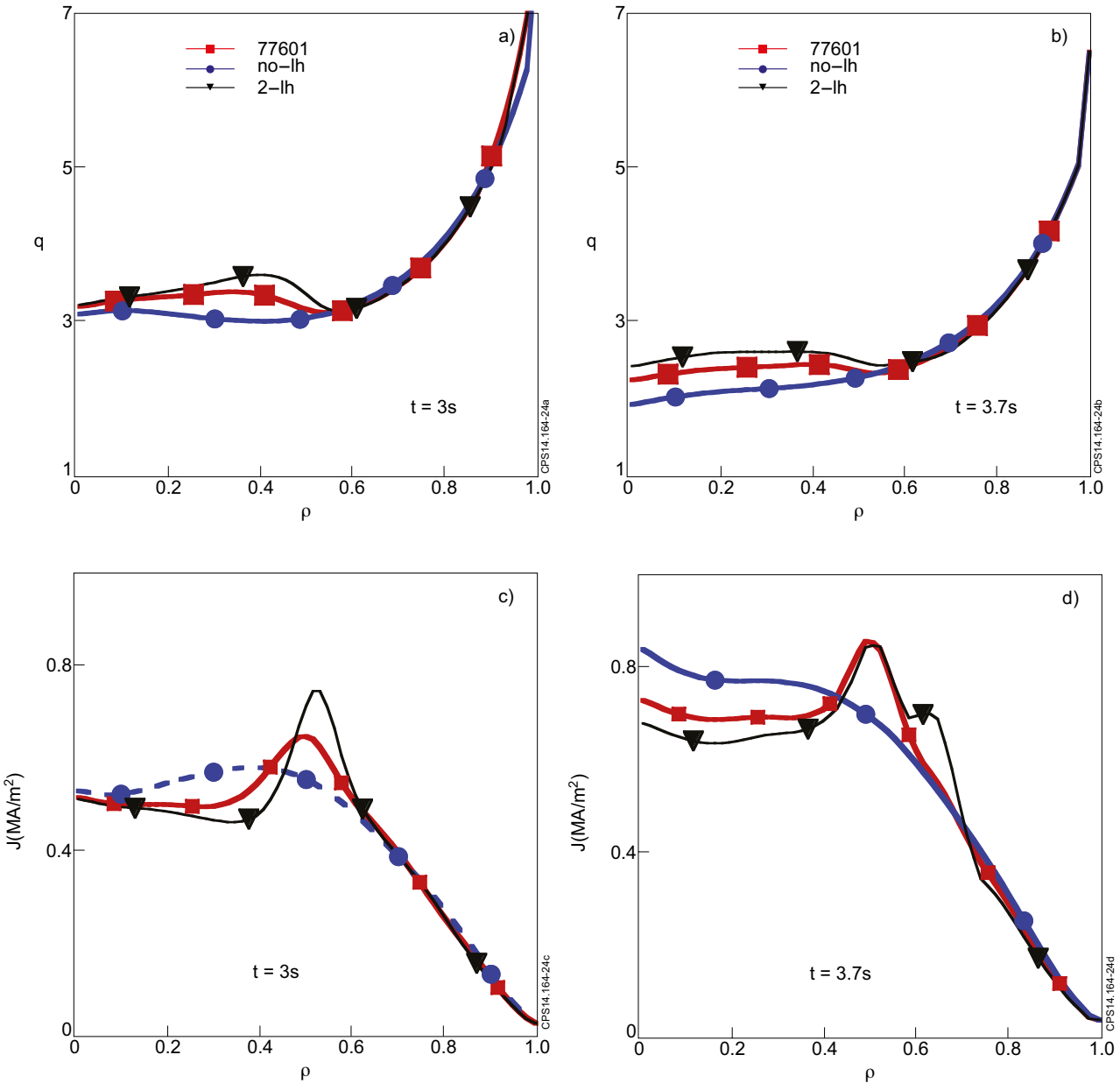

Figure 24: Effects of LHCD on q profile: q profiles for different LHCD efficiency: J_{LH} = 0 (blue circles), $\eta_{LH} = \eta_{LH\_FRTC}$ (red squares), η_{LH} = 2 η_{LH_FRTC} (black triangles), at t = 3s (a)) and at t = 3.7s (b)). Figure c) and d) show the corresponding plasma current density profiles while penetrating toward the plasma core.

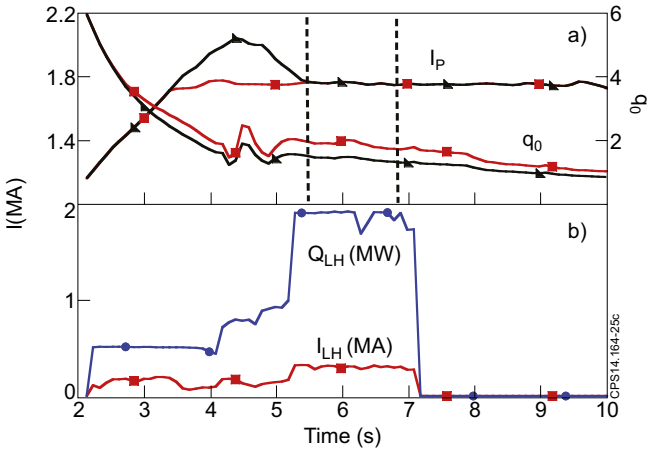

Figure 25: Hybrid scenario, comparison Overshoot/LHCD: a) plasma current (left scale) with overshoot (black triangles) and plasma current for LHCD (red squares) and temporal evolution of q_0 (right scale) for the two cases (same legend as I_P); b) LH absorbed power and driven current for the LHCD case ($n_{//}$ = 2.1).

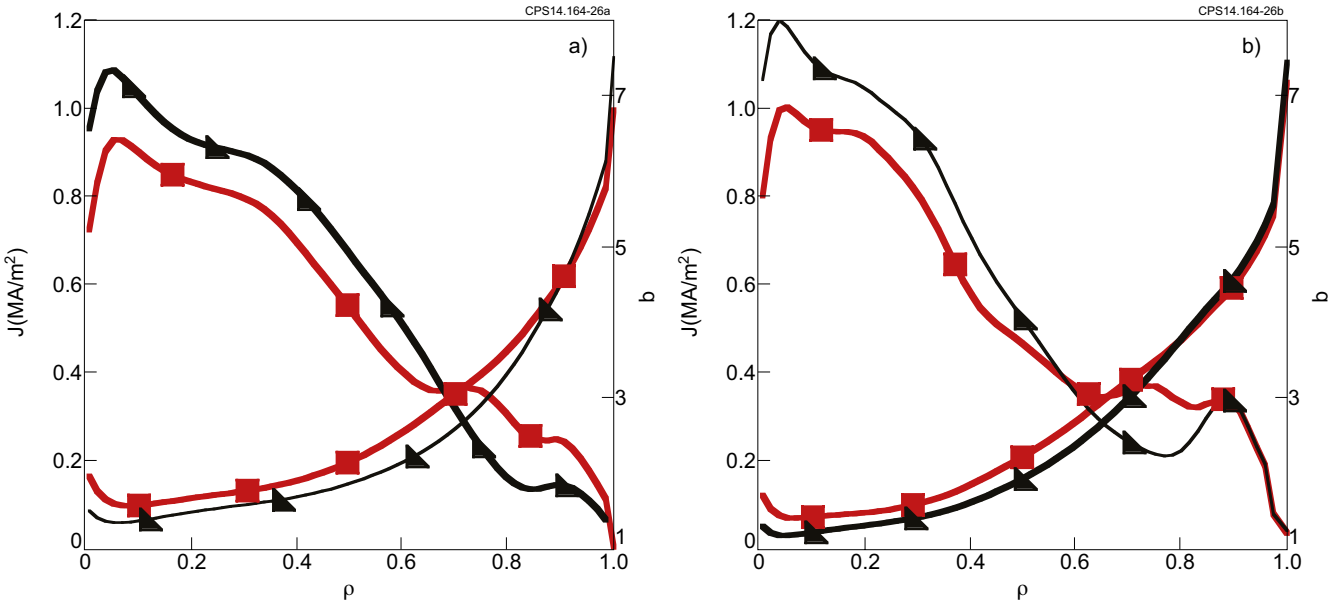

Figure 26: Hybrid scenario, comparison Overshoot/LHCD. J and q profiles for LHCD (red squares) and overshoot case (black triangles) are compared: a) at the end of the overshoot phase (t = 5.5s) and later on, b) at t = 6.8s.

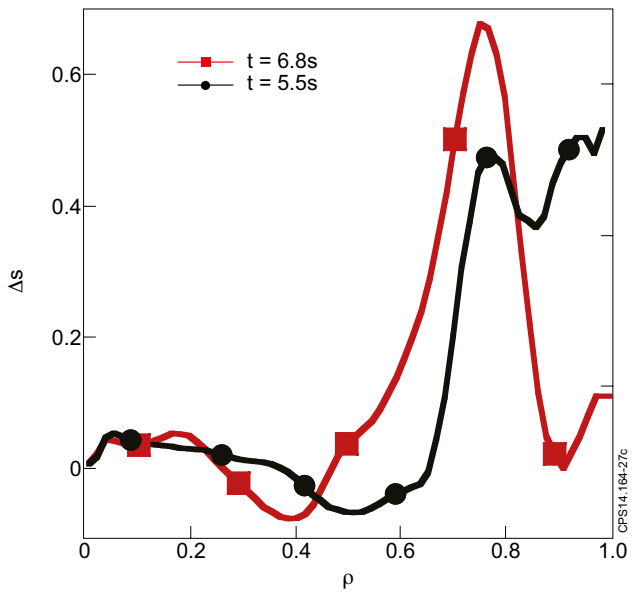

Figure 27: Hybrid scenario, comparison Overshoot/LHCD. The shear difference $\Delta s = s_{OV} - s_{LH}$ is shown vs. ρ. At t = 5.5s the difference is very small for ρ < 0.6 and grows in the interval 0.6 < ρ < 0.9; at t = 6.8s the difference is negligible for ρ < 0.5 and grows for ρ > 0.5.